2019 SCEC PROJECT REPORT

UCSB BROADBAND KINEMATIC RUPTURE SIMULATION WITH A DOUBLE CORNER SOURCE SPECTRUM

Principal Investigators: **Ralph Archuleta and Chen Ji**
Earth Research Institute
University of California, Santa Barbara

Abstract
In the UCSB method for computing broadband ground motion we explicitly specify a source spectrum. In the past, we have used a single corner Aki(1967)/Brune(1970) spectrum. However, using data from the NGA West-2 (Ancheta et al., 2014), we have determined that the spectrum should have two corners, one related to the overall duration and one related to the spectral level of the high frequency radiation. In essence, the classical Aki (1967)/Brune (1970) single-corner source spectrum should be modified to include a second corner, i.e., a double-corner frequency (DCF) source spectrum (e.g., Gusev, 1983; Luco, 1985; Atkinson, 1993; Atkinson and Silva, 1997).

Intellectual Merit
The classical Aki (1967)/Brune (1970) source spectrum has a single corner that can be related to stress drop (Brune, 1970, 1971). The single corner frequency is related to the overall duration of the rupture process. There is a stress parameter that controls the high frequencies which are directly related to root-mean-square acceleration (Hanks, 1979; McGuire and Hanks, 1980). There is clearly a difference in estimating the stress parameter from acceleration and stress drop estimated from a spectrum, assumed to have a single corner (Cotton et al., 2013). Using data from crustal earthquakes (Ancheta et al, 2014), we have determined scaling relations for the two corners of a double-corner source spectrum. This spectrum resolves the quandary discussed by Cotton et al. (2013) as to what is the stress drop of an earthquake.

Broader Impacts
A critical need for earthquake engineering is knowledge of near-source ground motion from damaging crustal earthquakes. While the data are becoming more plentiful (e.g., Ancheta et al., 2014), there is a notable lack of data within 20 km of the causative fault for earthquakes with M>6. Physics-based kinematic earthquake scenarios can provide computed broadband accelerograms for a wide range of magnitudes and distances.

Introduction

Because of a family emergency for both PI's, the project did not start on time. A no-cost extension to end of 2020 was requested and granted. Here we report our preliminary results in theory development and modification to the current UCSB broadband simulation algorithm.

1. Theory Development

We have introduced two double-corner frequency (DCF) source spectral models— JA19 and JA19_2S— for crustal earthquakes in active tectonic regimes (Ji and Archuleta, 2020). Both models have the shape defined as

$$\Omega_0(f, f_{c1}, f_{c2}) = \frac{M_0}{\left[1+(\frac{f}{f_{c1}})^4\right]^{1/4}\left[1+(\frac{f}{f_{c2}})^4\right]^{1/4}} \quad (1)$$

Model JA19 is self-similar. For 3.3<M<7.3, its corner frequencies f_{c1} and f_{c2} scale with magnitude M as

$\log(f_{c1}(M)) = 1.754 - 0.5M$

$\log(f_{c2}(M)) = 3.250 - 0.5M$

$\log(f_c^A(M)) = 2.502 - 0.5M.$ (2)

Here $f_c^A = \sqrt{f_{c1}f_{c2}}$ is an apparent single corner frequency (SCF) omega-squared model that fits low and high frequency asymptotical amplitudes of the JA19 model. The black lines in Figure 1a show the acceleration Fourier amplitude source spectra of M=5, and 7 earthquakes, predicted by JA19. This model satisfactorily fits the log-mean PGA, PGV and DomF as a function of magnitude for the NGA West-2 dataset from M 3.3 to M 7.3. However, the model notably underpredicts the observations around M 5.3. The source duration τ_d predicted by the JA19 model ($\tau_d = 1/\pi f_{c1}$) is in good agreement with the scaling relationships of the scaling relationship used by GCMT project [*Ekström et al.*, 2005] and that derived for non-subduction earthquakes [*Courboulex et al.*, 2016] The scaled energy (E_R/M_0) of the JA19 model is 2.2x10^{-5}, and the corresponding apparent stress drop $\Delta\sigma_a$ is 0.73 MPa. Both are in good agreement with the previous results [*Ide and Beroza*, 2001]. The relative amplitudes of E_R in three frequency bands, $f \leq f_{c1}$, $f_{c1} < f < f_{c2}$ and $f \geq f_{c2}$ are 0.5%, 49.0%, and 50.5%, respectively.

Aiming to resolve the misfit around M 5.3, we modified the scaling relation of f_{c1} in the JA19 model and obtain a two-segment scaling relationship,

$$\log(f_{c1}) = \begin{cases} 1.4735 - 0.415\,M & M \leq 5.3 \\ 2.3745 - 0.585\,M & M > 5.3 \end{cases} \quad (3)$$

The scaling relation of f_{c2} is the same as in Equation 2. We name this model JA19_2S accordingly. This work was conducted under the support of the current grant. JA19_2S explains the log-mean PGA, PGV and DomF of NGA West-2 dataset from M 3.3 to M 7.3 remarkably well (Figure 1). Considering the relation $\tau_d = 1/\pi f_{c1}$, the source duration τ_d inferred from JA19_2S increases with seismic moment as ${M_0}^{1/(3+\varepsilon)}$, with $\varepsilon \sim 0.614$ for 3.3<M<5.3 and $\varepsilon \sim -0.436$ for 5.3<M<7.3. Because of $M_0 \propto (\Delta\sigma_s {V_r}^3){\tau_d}^3$ [e.g., *Kanamori and Rivera*, 2004], this may suggest:

(1) $\Delta\sigma_s$ is a constant but the rupture velocity V_r increases 47% when magnitude increases from M 3.3 to M 5.3 and subsequently decrease 47% when magnitude further increases to 7.3.
(2) V_r is a constant but the average stress drop $\Delta\sigma_s$ increases 3.2 times when magnitude increases

from M 3.3 to M 5.3 and subsequently decreases 3.2 times when magnitude further increases to 7.3. This is analogous to what *Atkinson and Silva* [1997] found.

In both cases, the scaled energy increases 2.2 times from 2.2×10^{-5} for M 3.3 events to 4.7×10^{-5} for M 5.3 events, and subsequently decreases 2.2 times to 2.2×10^{-5} for M 7.3 events.

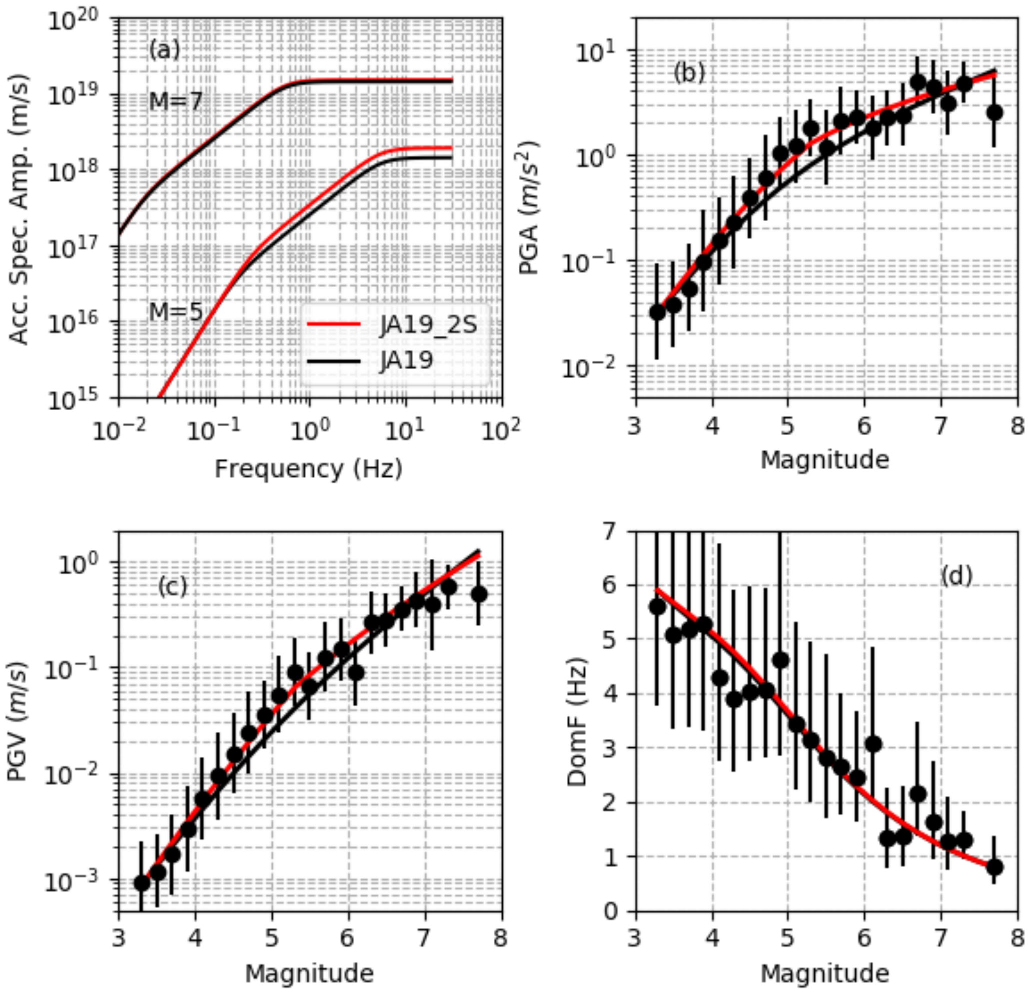

Figure 1. Comparison of DCF JA19 and JA19_2S models. (a) Comparison of synthetic acceleration Fourier amplitude spectra of M 5 and 7 earthquakes, predicted by JA19 and JA19_2S models. The comparisons of the synthetic (red line for JA19_2S and black line for JA19) and observed log-mean PGA, PGV, and DomF values (black circles) are shown in (b), (c), and (d), respectively. The bars denote the corresponding standard deviations.

2. Modification of UCSB broadband simulation method

In the current UCSB broadband simulation method [*Crempien and Archuleta*, 2015; *Liu et al.*, 2006; *Schmedes et al.*, 2013] there is an explicit constraint: the final moment-rate spectrum should approximate an Aki-Brune single corner spectrum that has an a priori corner based on an assumed stress drop. (The temporal parameters related to the rupture time and the slip-rate functions of each subfault are continuously adjusted in an inner loop until the spectrum of source moment-rate function approximates a specified Aki-Brune spectrum). The main subject we had proposed is to replace the single corner spectrum with a DCF model similar to JA19 in Ji and Archuleta (2020).

Figure 2 shows a representative result using the 1999 Hector Mine earthquake as an example. Using a moment magnitude of 7.13 [*Ji et al.*, 2002] in Equation (2), we obtain the double corner frequencies (f_{c1}, f_{c2}) of (0.015 Hz, 0.48 Hz). The apparent SCF corner frequency f_c^A is 0.085 Hz. The Hector Mine earthquake had been studied during the code validation with UCSB method. The optimal corner frequency f_c of the Brune spectrum found during previous trial-and-error studies was 0.075 Hz. The predicted f_c^A agrees with this optimal f_c remarkably well. In this experiment, we try to find an optimal source model with an acceleration spectral shape in the frequency band from 0.2 Hz to 20 Hz that is similar to that of JA19 model.

Without loss of generality, let's represent the normalized moment rate function as $M_0(t_k), t_k = (k-1)*dt, k = 1,2, \ldots 2^N$, dt is sampling interval. Its acceleration spectrum is $4\pi^2\widetilde{M}_0(f_k), f_k = (k-1)*df, k = 1,2, \ldots 2^{N-1}$. f_k varies from zero to $2^{N-1}df$ $(df = 1/2^N dt)$. We divide the entire frequency range into N-1 bands. The frequency range of an arbitrary band m (m=1, 2, …N-1) is $[2^{m-1}df, (2^m - 1)df]$. We have estimated the geometric mean of the spectrum within each band. The yellow dots in Figures 2b-2d denote the centers of these frequency bands and corresponding geometric means. During the inversion, we minimize these mean spectral values estimated from JA19 model and potential source model. Using this approach, we can avoid over-weighting the high frequency signals. Figure 2a shows the normalized moment rate function of one optimal source model. Figure 2c-2d shows corresponding displacement, velocity and acceleration spectrum as a black line, accompanying with the JA19 model in red line. Note that the yellow dots match the JA19 model well.

Regardless the success shown in Figure 2, we have found a caveat that was previously overlooked. The average rise time (simple average) of this optimal source model is only 0.4 s, which is small for such an M 7 earthquake. We have reviewed the previous realizations using the single-corner frequency source spectra as the constraint, and found similar results. *Somerville et al.* [1999] analyzed about 20 finite fault slip models and found that the average rise time T_R of an earthquake scales with seismic moment as $T_R = 2.03 \times 10^{-9} M_0^{1/3}$, M_0 in dyne.cm. The predicted average rise time for the 1999 Hector Mine earthquake is 1.7 s, over 4 times larger than found in our source model. The finite fault inversions have mainly relied on the seismic data with frequency less than 1.0 Hz; the inverted rise time might be overestimated to some extent. Based on the results of the strong ground motion validation tests, *Graves and Pitarka* [2015] suggested a modified empirical relationship. For a vertical strike-slip fault, they found that the average rise time satisfies $T_R = 1.45 \times 10^{-9} M_0^{1/3}$, M_0 in dyne.cm. With this relation the expected average rise time T_R for a M 7.13 earthquake is 1.2 s, still a factor of three larger than ours. The fact that optimal source model has a short rise time suggests that the models with appropriate average rise time cannot excite enough high frequency signals. Resolving this issue has become our highest priority; we are looking into many different remedies.

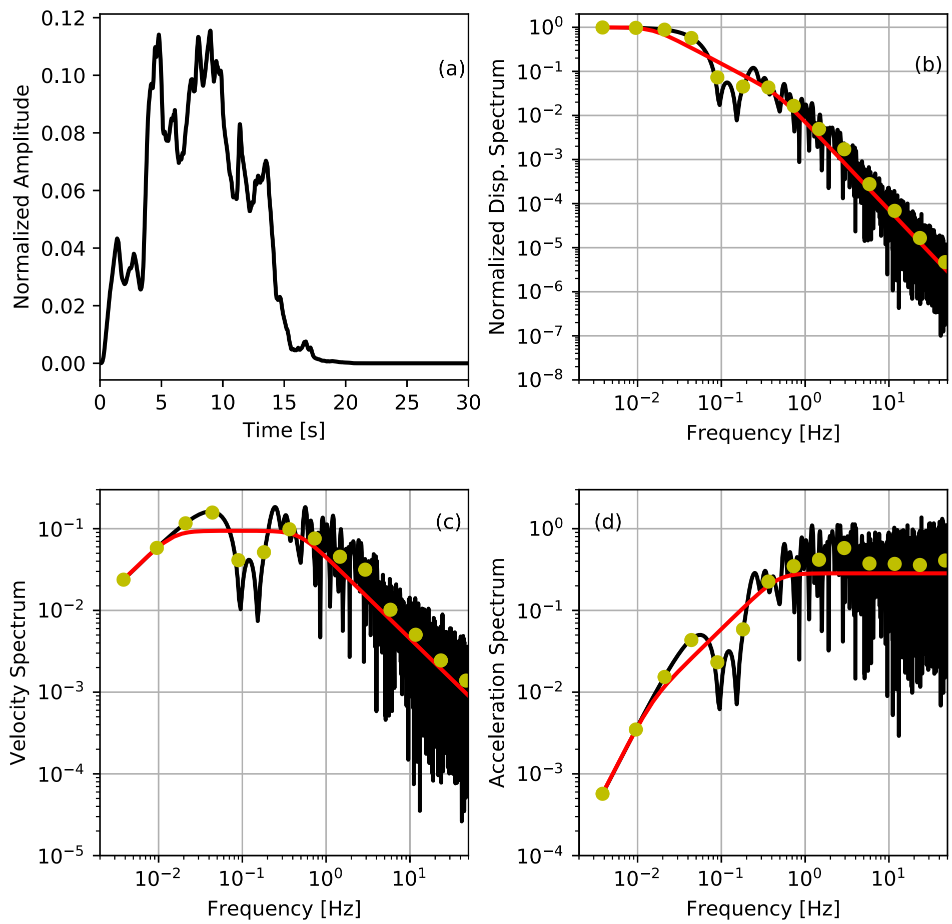

Figure 2. Moment rate function of one realization of M 7.13 Hector Mine earthquake (a) and its corresponding normalized spectrum in displacement (b), velocity (c) and acceleration (d) in black line. The red line in Figure b-d shows the double-corner frequency spectrum predicted using model JA19. We divide the spectra into multiple frequency bands. The yellow dots denote the centers of these frequency bands the geometric means of spectral values within these bands. The dots within the frequency range from 0.2 Hz to 22.5 Hz shall match the red line. See text for details.

Reference

Aki, K. (1967), Scaling law of seismic spectrum. *J Geophys. Res.* **72**, 1217-1231.

Ancheta, T. D., R. B. Darragh, J. P. Stewart, E. Seyhan, W. J. Silva, B. S.-J. Chiou, K. E. Wooddell, R. W. Graves, A. R. Kottke, D. M. Boore, T. Kishida and J. L. Donahue (2014), NGA-West2 database, *Earthquake Spectra* **30**, 989–1005.

Atkinson, G. M. (1993), Earthquake source spectra in eastern North America, *Bull. Seismol. Soc. Am.* **83**, 1778-1798.

Atkinson, G. M., and W. Silva (1997), An empirical study of earthquake source spectra for California earthquakes, *B Seismol Soc Am*, *87*(1), 97-113.

Brune, J. N. (1970), Tectonic stress and spectra of seismic shear waves from earthquakes. *J. Geophys. Res.* **75**, 4997-5009. Correction, (1971), Ibid. 76, 5002.

Cotton, F., R. J. Archuleta and M. Causse (2013), What is the sigma of stress drop?, *Seismol. Res. Lett.* **84**, 42-48, doi: 10.1785/0220120087

Courboulex, F., M. Vallee, M. Causse, and A. Chounet (2016), Stress-Drop Variability of Shallow Earthquakes Extracted from a Global Database of Source Time Functions, *Seismological Research Letters*, *87*(4), 912-918, doi:10.1785/0220150283.

Crempien, J. G. F., and R. J. Archuleta (2015), UCSB Method for Simulation of Broadband Ground Motion from Kinematic Earthquake Sources, *Seismological Research Letters*, *86*(1), 61-67, doi:10.1785/0220140103.

Ekström, G., A. M. Dziewoński, N. N. Maternovskaya, and M. Nettles (2005), Global seismicity of 2003: centroid–moment-tensor solutions for 1087 earthquakes, *Phys Earth Planet In*, *148*(2-4), 327-351, doi:10.1016/j.pepi.2004.09.006.

Graves, R., and A. Pitarka (2015), Refinements to the Graves and Pitarka (2010) Broadband Ground-Motion Simulation Method, *Seismological Research Letters*, *86*(1), 75-80, doi:10.1785/0220140101.

Gusev, A. A. (1983), Descriptive statistical-model of earthquake source radiation and its application to an estimation of short-period strong motion. *Geophys. J. Roy. Astr. Soc.* **74**, 787-808 (1983).

Hanks, T. C. (1979). b-Values and γ^{-n} source models: implications for tectonic stress variations along crustal fault zones and the estimation of high frequency strong ground motion, *J. Geophys. Res.* **84**, 2235-2242.Ide, S., and G. C. Beroza (2001), Does apparent stress vary with earthquake size?, *Geophys Res Lett*, *28*(17), 3349-3352, doi:Doi 10.1029/2001gl013106.

Ji, C., D. J. Wald, and D. V. Helmberger (2002), Source description of the 1999 Hector Mine, California, earthquake, part II: Complexity of slip history, *Bull Seismol Soc Am*, *92*(4), 1208-1226, doi:Doi 10.1785/0120000917.

Kanamori, H., and L. Rivera (2004), Static and dynamic scaling relations for earthquakes and their implications for rupture speed and stress drop, *Bull Seismol Soc Am*, *94*(1), 314-319.

Liu, P. C., R. J. Archuleta, and S. H. Hartzell (2006), Prediction of broadband ground-motion time histories: Hybrid low/high-frequency method with correlated random source parameters, *Bull. Seismol Soc Am*, *96*(6), 2118-2130, doi:10.1785/0120060036.

Luco, J. E. (1985), On strong-ground motion estimates based on models of the radiated spectrum, *Bull Seismol Soc Am* 75, 641-649.

McGuire, R. K., and T. C. Hanks (1980). RMS accelerations and spectral amplitudes of strong motion during the San Fernando earthquake, *Bul. Seismol Soc Am* **70**, 1907–1920.

Schmedes, J., R. J. Archuleta, and D. Lavallee (2013), A kinematic rupture model generator incorporating spatial interdependency of earthquake source parameters, *Geophys J Int*, *192*(3), 1116-1131, doi:10.1093/gji/ggs021.

Somerville, P., K. Irikura, R. Graves, S. Sawada, D. Wald, N. Abrahamson, Y. Iwasaki, T. Kagawa, N. Smith, and A. Kowada (1999), Characterizing Crustal Earthquake Slip Models for the Prediction of Strong Ground Motion, *Seismological Research Letters*, *70*(1), 59-80, doi:10.1785/gssrl.70.1.59.